© 2020. Published by The Company of Biologists Ltd | Development (2020) 147, dev193094. doi:10.1242/dev.193094

RESEARCH ARTICLE

The vascular endothelial cell-expressed prion protein doppel promotes angiogenesis and blood-brain barrier development

Zhihua Chen[1], John E. Morales[1], Naze Avci[1], Paola A. Guerrero[1], Ganesh Rao[1], Je Hoon Seo[2] and Joseph H. McCarty[1,*]

ABSTRACT

The central nervous system (CNS) contains a complex network of blood vessels that promote normal tissue development and physiology. Abnormal control of blood vessel morphogenesis and maturation is linked to the pathogenesis of various neurodevelopmental diseases. The CNS-specific genes that regulate blood vessel morphogenesis in development and disease remain largely unknown. Here, we have characterized functions for the gene encoding prion protein 2 (*Prnd*) in CNS blood vessel development and physiology. *Prnd* encodes the glycosylphosphatidylinositol (GPI)-linked protein doppel, which is expressed on the surface of angiogenic vascular endothelial cells, but is absent in quiescent endothelial cells of the adult CNS. During CNS vascular development, doppel interacts with receptor tyrosine kinases and activates cytoplasmic signaling pathways involved in endothelial cell survival, metabolism and migration. Analysis of mice genetically null for *Prnd* revealed impaired CNS blood vessel morphogenesis and associated endothelial cell sprouting defects. $Prnd^{-/-}$ mice also displayed defects in endothelial barrier integrity. Collectively, these data reveal novel mechanisms underlying doppel control of angiogenesis in the developing CNS, and may provide new insights about dysfunctional pathways that cause vascular-related CNS disorders.

KEY WORDS: Vascular basement membrane, Microenvironment, Neurovascular unit, Extracellular matrix, Astrocyte, Barriergenesis

INTRODUCTION

The CNS is the most vascularized organ system in the human body (Tam and Watts, 2010). Its billions of neurons and glia interact with blood vessels within multicellular complexes or neurovascular units (NVUs) that regulate angiogenesis (Tata et al., 2015) and homeostasis of endothelial barrier integrity (Zhao et al., 2015). Growth factors, extracellular matrix (ECM) proteins and their cognate cell surface receptors regulate communication between cells of the NVU in a coordinated manner to promote normal CNS development and physiology (Paredes et al., 2018). For example, vascular endothelial growth factor-A (VEGF-A) and its receptor tyrosine kinase VEGFR2 are crucial for promoting endothelial cell proliferation, survival and sprouting in the CNS (Nakayama et al., 2013). VEGF-dependent angiogenesis in the developing CNS is linked to activation of Notch-Dll4 signaling in vascular endothelial tip cells (Jakobsson et al., 2009; Siekmann et al., 2008). VEGF-A signaling is also linked to Slit signaling through Robo receptors and is crucial for developmental CNS angiogenesis (Rama et al., 2015). Furthermore, the Slit2-Robo complex in endothelial cells is involved in VEGFR2 internalization and signaling (Genet et al., 2019). Integrin-mediated activation of TGF-β signaling is also crucially involved in control of sprouting angiogenesis and NVU development (Arnold et al., 2014; Hirota et al., 2015, 2011; Ma et al., 2017; McCarty, 2020; Mobley et al., 2009). In addition, Wnts secreted by radial glial cells also promote angiogenesis and blood-brain barrier (BBB) formation (Stenman et al., 2008) via activation of β-catenin and other pathways in CNS endothelial cells (Liebner et al., 2008). GPR124, an atypical G protein-coupled receptor expressed in endothelial cells that is essential for CNS angiogenesis (Kuhnert et al., 2010; Posokhova et al., 2015), acts in combination with Reck in a multicomplex to promote Wnt-dependent β-catenin activation (Vanhollebeke et al., 2015). Cross-talk between TGF-β and Wnt signaling effectors are important for normal angiogenesis and endothelial barrier maturation (Jensen et al., 2019). Reelin signaling via Dab1 in vascular endothelial cells is also crucial for neurovascular development (Segarra et al., 2018). Pericyte recruitment to CNS endothelial cells via the platelet-derived growth factor B (PDGFB)-PDGFRβ signaling axis is also important for induction of blood vessel stability and BBB formation (Daneman et al., 2010). Aberrant expression or function of components of the above-mentioned pathways is linked to the onset of various disorders related to CNS angiogenesis, including germinal matrix hemorrhage (Brouwer et al., 2014), white matter leukoencephalopathy (Haynes et al., 2013) and retinopathy of prematurity (Swan et al., 2018), as well as adult-onset brain diseases including cancer (Lathia et al., 2015). Additional regulatory components and pathways that control angiogenesis and NVU development, and how they might be linked to the VEGF, TGFβ and/or Wnt signaling components in CNS vascular development and disease, remain largely uncharacterized.

In mice, the prion family consists of the canonical cellular prion protein (Prp^c) and the prion-like proteins shadoo and doppel (also known as prion protein 2 and Prnd) (Ciric and Rezaei, 2015; Watts and Westaway, 2007). Prp^c is highly expressed throughout the adult brain, where it interacts with co-receptors and extracellular ligands to promote neuronal survival (Didonna, 2013). Mutated or misfolded Prp^c generates extracellular plaques that cause irreversible neurodegenerative disorders such as spongiform encephalopathy in cattle and Creutzfeldt-Jakob disease in humans (Prusiner et al., 1988). Genetic studies in mice have demonstrated that endogenous Prp^c in neurons is essential for the pathogenesis of prion disease, with deletion of the Prp^c gene (*Prnp*) promoting resistance to inoculated prions (Prusiner et al., 1993). Characterization of genomic regions flanking mouse *Prnp* led to the discovery of *Prnd*, a closely linked prion-like gene that encodes the doppel protein. *Prnd* is just 15 kb

[1]Department of Neurosurgery, University of Texas M. D. Anderson Cancer Center, Houston, TX 77030, USA . [2]Department of Anatomy, Chungbuk National University College of Medicine, Chungbuk 28644, Republic of Korea.

*Author for correspondence (jhmccarty@mdanderson.org)

J.H.M., 0000-0002-8345-5478

Handling Editor: James Briscoe
Received 19 May 2020; Accepted 17 August 2020

Development (2020) 147, dev193094. doi:10.1242/dev.193094

downstream of *Prnp* on mouse chromosome two and 20 kb away on human chromosome 20 (Silverman et al., 2000). Doppel has a predicted molecular weight of 20 kDa and is similar to Prp^c in that it undergoes a C-terminal glycosylphosphatidylinositol (GPI) modification and has at least two N-glycosylation sites. The apparent molecular weight of doppel after post-translation modification is 30-50 kDa (Silverman et al., 2000). Doppel and Prp^c share just 20% sequence identity, mainly within three common α-helical-rich or 'prion domains' (Lührs et al., 2003).

Prnd mRNA is highly expressed in the testes and in the brain during embryonic and neonatal development. Interestingly, *in situ* hybridization experiments reveal that *Prnd* mRNA is expressed mainly within vascular cells of angiogenic blood vessels in the developing brain, with expression peaking in the early post-natal period and diminishing in the adult brain when blood vessels become quiescent and cease proliferating and sprouting (Li et al., 2000). Transgenic overexpression of *Prnd* in cerebellar neurons of $Prnp^{-/-}$ mice leads to progressive cerebellar neurodegeneration, and these pathologies can be rescued by expression of *Prnp* (Moore et al., 2001). Genetic ablation of the *Prnd* gene in mice does not lead to any obvious neurological or vascular pathologies that have been reported. $Prnd^{-/-}$ mice are postnatal viable and females are fertile, although mutant males are sterile due to spermatogenesis defects (Paisley et al., 2004). Unlike Prnp, heritable mutations in PRND have not been reported in humans, and there is little direct evidence that doppel forms aggregates that promote pathogenesis of prion-related diseases (Mastrangelo and Westaway, 2001).

Here, we report that doppel is essential for normal control of angiogenesis during CNS development and has links to pathological angiogenesis. Biochemical assays and primary endothelial cell culture systems reveal that GPI-linked doppel activates transmembrane receptor tyrosine kinases with central roles in blood vessel survival, metabolism and migration. Genetic ablation of *Prnd* in mice leads to defective blood vessel morphogenesis associated with impaired endothelial tip cell polarity and sprouting in the developing brain and retina. $Prnd^{-/-}$ mice also display defects in brain endothelial barrier integrity. Collectively, these results reveal novel functions for the prion protein family member doppel in CNS blood vessel morphogenesis and maturation, and suggest that targeting doppel to block angiogenesis could be an effective therapeutic approach to treat vascular-related CNS pathologies.

RESULTS

To characterize new regulatory factors involved in CNS blood vessel morphogenesis and physiology, we mined open source databases to identify genes that are (i) enriched in angiogenic endothelial cells during CNS development, (ii) downregulated in quiescent endothelial cells in the adult CNS and (iii) upregulated in angiogenic endothelial cells in CNS pathologies. As shown in Fig. 1A, analysis of the brain RNA sequencing (RNA-seq) database, in which various cells types from the neonatal mouse brain were fractionated and the differential gene expression quantified using RNA-seq, revealed that *Prnd* mRNA is expressed exclusively in brain vascular endothelial cells. Analysis of the genepaint.org database (Visel et al., 2004), which catalogs spatial patterns of gene expression in the developing mouse brain, confirmed *Prnd* mRNA in brain blood vessels (Fig. 1B). Quantitative RT-PCR strategies were then used to analyze temporal expression levels of *Prnd* mRNA in the developing and mature mouse brain. We detected relatively high levels of *Prnd* mRNA expression between neonatal ages postnatal day one (P1) and P3 (Fig. 1C). *Prnd* mRNA expression levels showed a decrease after P7 and low levels in the mouse brain at P21 and later adult ages (Fig. 1C). These results are consistent with a prior report showing that *Prnd* mRNA expression peaks in the neonatal mouse brain (Li et al., 2000). In contrast, *Prnp*

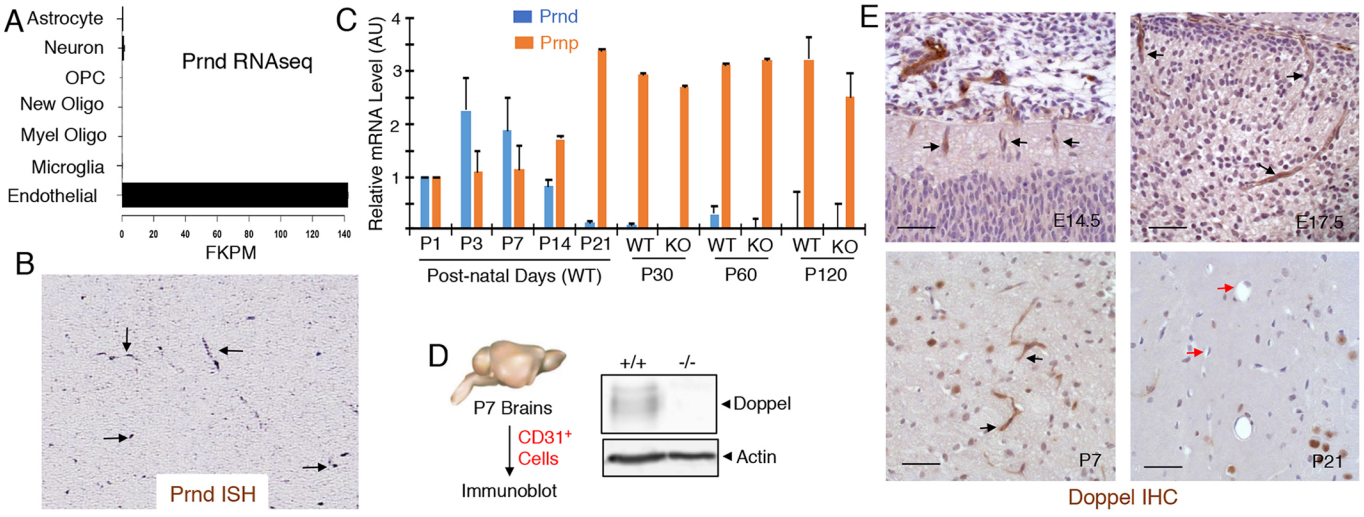

Fig. 1. Doppel is expressed in vascular endothelial cells of angiogenic blood vessels in the developing brain. (A) Analysis of the brain RNA-seq database reveals that *Prnd* mRNA is expressed exclusively in brain endothelial cells isolated from Tie2-GFP mice at P7. The expression data were graphed as fragments per kb of transcript per million (FKPM). (B) Analysis of the genepaint.org database reveals *Prnd* mRNA expression in blood vessels of the E14.5 embryonic mouse brain (black arrows). (C) Quantitation of *Prnp* and *Prnd* mRNA levels in the total mouse brain at different postnatal ages using qRT-PCR. Note that *Prnd* mRNA levels in the neonatal brain are reduced after P7 and are very low in the adult mouse brain. *Prnd* mRNA is absent in the adult $Prnd^{-/-}$ mouse brain. Differences in *Prnp* mRNA levels between wild-type and $Prnd^{-/-}$ adult brain samples are not statistically significant. (D) $CD31^+$ vascular endothelial cells were fractionated from *Prnd* wild-type ($^{+/+}$) or *Prnd* knockout ($^{-/-}$) neonatal mouse brains (P7) and doppel protein expression was determined by immunoblotting. Note the absence of doppel expression in the $Prnd^{-/-}$ brain endothelial cell fractions. (E) Sagittal sections from wild-type brain tissue from different embryonic (14.5 and E17.5) and postnatal (P7 and P21) ages were immunohistochemically labeled with anti-doppel antibodies. Note that doppel is expressed in vascular endothelial cells of the embryonic and neonatal brains (black arrows) but is reduced in the more mature P21 brain (red arrows). Scale bars: 50 µm.

Development (2020) 147, dev193094. doi:10.1242/dev.193094

mRNA levels were relatively low in the neonatal brain but showed an increase with age, with highest levels detected in the adult brain. *Prnp* mRNA levels were not significantly different in *Prnd*$^{-/-}$ brain samples (Fig. 1C). Next, to analyze doppel protein expression we generated a rabbit polyclonal antibody directed against an N-terminal human doppel peptide sequence that shares 100% sequence identity with mouse doppel. Antibody specificity for mouse and human doppel was confirmed by immunoblotting tissue and cell lysates (Fig. S1). Neonatal mouse brains were used as a source to fractionate primary vascular endothelial cells based on expression of CD31 (also known as Pecam1). As shown in Fig. 1D, we detected doppel expression in CD31-positive endothelial cells isolated from neonatal mouse brains. Anti-doppel immunohistochemistry revealed protein expression in sprouting blood vessels of the embryonic mouse brain as early as E14.5 and expression persisted to later embryonic stages (Fig. 1E). Doppel expression was also detected in blood vessels in the neonatal brain at P7. Consistent with the *Prnd* mRNA data (Fig. 1C), doppel protein expression was diminished in most blood vessels at P21 (Fig. 1E). Specificity of the anti-doppel antibody used for immunohistochemistry and immunoblotting was confirmed using tissue and lysates from wild-type and *Prnd* homozygous null (*Prnd*$^{-/-}$) mice (Fig. S2).

Given that doppel levels are high in angiogenic blood vessels of the developing mouse brain but diminished in quiescent blood vessels of the adult brain, we next asked whether doppel expression was reactivated in endothelial cells during pathological angiogenesis. Analysis using the Ivy glioblastoma (GBM) atlas project (Ivy-GAP), which contains spatial characterization of genes expressed in different regions of the highly vascularized malignant brain cancer GBM, revealed *PRND* mRNA expression mainly within areas of microvascular proliferation (Fig. S3A). In confirmation of the vascular endothelial cell expression patterns shown for PRND in human GBM, analysis of other human tumor samples within the cBioportal database revealed that *PRND* mRNA is highly coexpressed with several well-characterized vascular endothelial cell markers such as CDH5, DLL4 and PECAM1 (Fig. S3B).

Next, we analyzed doppel functions in vascular endothelial cells *in vitro*. Primary human umbilical vein endothelial cells (HUVECs) and human brain microvascular endothelial cells (HBMECs) were tested for endogenous levels of doppel. Endogenous expression was not detected as determined by immunoblotting (Fig. S4 and Fig. 2). Therefore, we used recombinant lentiviruses (pLOC-PRND) to express doppel in HBMECs. Doppel expression and N-glycosylation were detected in pLOC lentivirus-infected brain endothelial cells (Fig. 2A,B). Similar results were detected after expression of doppel in non-neural primary vascular endothelial cultures such as HUVECs (Fig. S4). Analysis of cell viability and invasion *in vitro* revealed that lentiviral-mediated doppel expression resulted in reduced brain endothelial cell viability (Fig. 2C) but increased in invasion through the three-dimensional ECM (Fig. 2D). In contrast, forced expression of doppel in HUVECs did not result in reduced viability (Fig. S4E). To analyze potential doppel-mediated signaling functions in brain endothelial cells, we utilized reverse-phase protein array (RPPA), which is an antibody-based high-throughput system to study protein signaling cascades (Nishizuka and Mills, 2016). Several signaling effectors involved in endothelial cell growth and migration, such as Akt and Src, are differentially expressed and/or

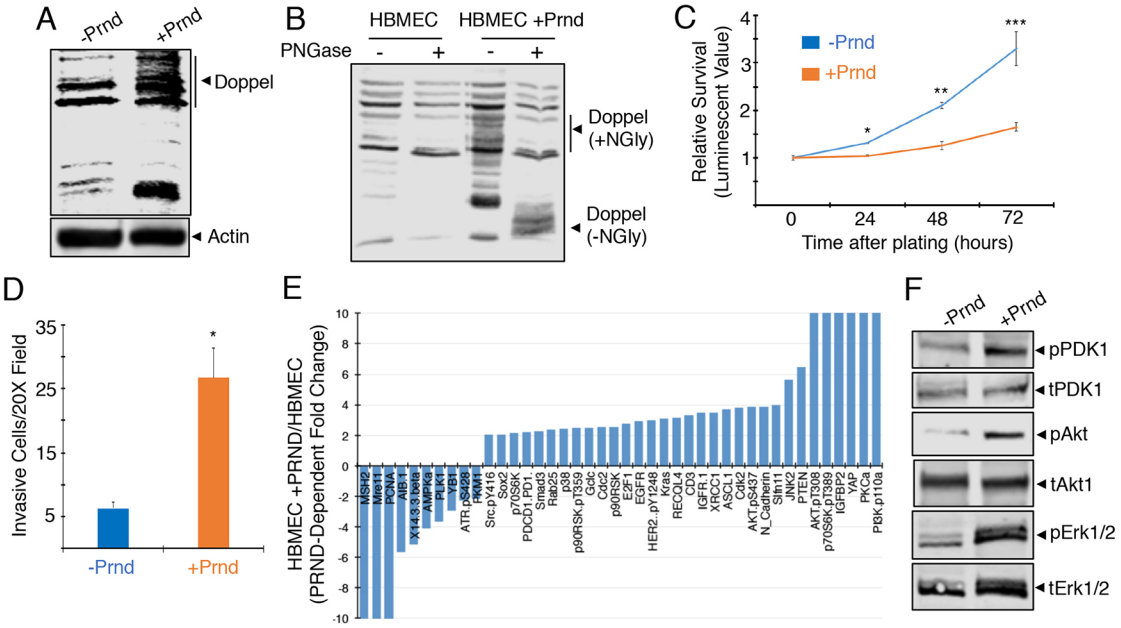

Fig. 2. Doppel activates cytoplasmic angiogenic signaling pathways in brain endothelial cells. (A) HBMECs were infected with control pLOC lentivirus or pLOC expressing PRND. Blot shows validation of doppel expression in HBMECs infected with control pLOC or pLOC-PRND by immunoblotting of detergent-soluble lysates with an anti-doppel antibody. The bands detected in the HBMEC control lysate sample (−Prnd/doppel) are probably proteins nonspecifically recognized by the anti-doppel antibody or perhaps low levels of doppel or another prion protein. (B) Detergent-soluble lysates from HBMECs expressing doppel were treated with PNGase to remove N-linked oligosaccharides. Note that PNGase-mediated cleavage of N-linked oligosaccharides leads to an obvious decrease in the apparent molecular weight of doppel. (C) Viability of cultured HBEC-5i cells infected with control pLOC and pLOC-PRND were quantified every 24 h for 3 days; **P*<0.0001, ***P*=0.0001, ****P*=0.0016. (D) HBMECs were infected with control pLOC or pLOC-PRND and invasion was quantified after 24 h using three-dimensional ECM transwell assays; **P*=0.0001. (E) Summary of select proteins that show twofold or greater difference in expression and/or phosphorylation in control HBMECs or HBMECs expressing doppel. (F) Confirmation of doppel-activated signaling pathways by immunoblotting HBMEC lysates with phosphospecific signaling antibodies. Note the doppel-dependent increases in the phosphorylation of Pdk1, Akt and Erk1/2 proteins, as revealed by immunoblotting detergent-soluble HBMEC lysates with phosphospecific antibodies. Differences among groups were analyzed using one-way ANOVA.

Development (2020) 147, dev193094. doi:10.1242/dev.193094

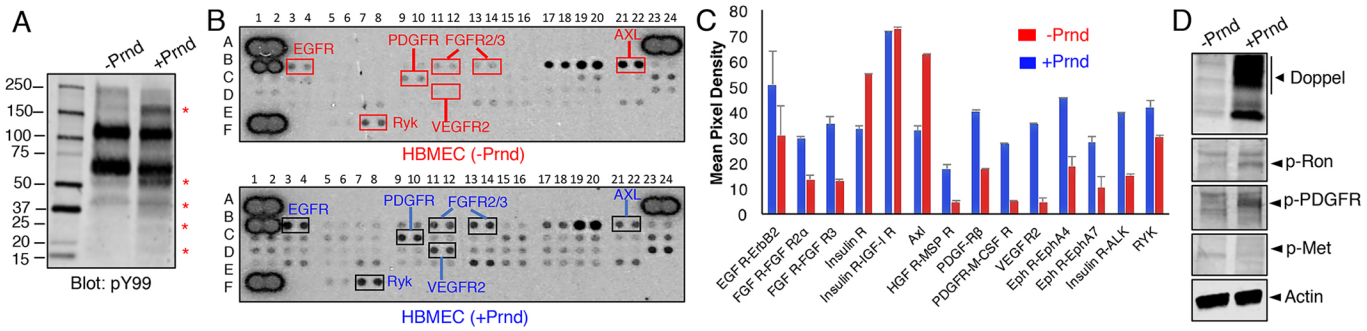

Fig. 3. Doppel activates angiogenic receptor tyrosine kinase signaling in brain endothelial cells. (A) Lentiviral-mediated expression of doppel in HBMECs correlates with higher levels of tyrosine-phosphorylated proteins, as revealed by anti-phosphotyrosine immunoblotting. Asterisks indicate proteins that show higher levels of tyrosine phosphorylation in cells expressing doppel. (B) Detergent-soluble lysates from control HBMECs (top array) or HBMECs expressing doppel (bottom array) were used to probe phospho-RTK arrays, revealing doppel-dependent increases in phosphorylation of select RTKs. (C) Doppel-dependent differences in select RTK phosphorylation levels based on densitometry-based scan of the array data shown in B. (D) Doppel-dependent tyrosine phosphorylation of RTKs in HBMECs was confirmed by immunoblotting with various phosphospecific antibodies recognizing Ron, PDGFRα/β and c-Met. Differences among groups were analyzed using one-way ANOVA.

phosphorylated in a doppel-dependent manner in HBMECs (Fig. 2E; Fig. S5). Doppel expression results in the increased phosphorylation of select signaling factors identified from RPPA (including Pdk1, Akt and Erk1/2) and was confirmed by immunoblotting detergent-soluble lysates from HBMECs using phosphospecific antibodies (Fig. 2F).

Expression of doppel in HBMECs stimulates the tyrosine phosphorylation of several proteins (Fig. 3A). Because doppel is a GPI-linked surface protein and lacks an intracellular signaling domain, we surmised that there are functional links between doppel and transmembrane proteins with intracellular enzymatic activities, including growth factor receptor tyrosine kinases (RTKs). Therefore, lysates from control HBMECs or HBMECs expressing doppel were tested in commercially available antibody filter arrays designed to detect tyrosine phosphorylation epitopes on various RTKs, including some with links to CNS angiogenesis. Doppel-dependent increases in the tyrosine phosphorylation of several RTKs were detected, including many RTKs with established functions in angiogenesis such VEGFR2, PDGFRα/β and FGFR (Fig. 3B,C). Phosphospecific antibodies were used to confirm doppel-dependent increases in RTK tyrosine phosphorylation levels in HBMECs infected with pLOC-PRND (Fig. 3D). Interactions between doppel and VEGFR2 in brain endothelial cells were confirmed using proximity ligation assays (Fig. 4A-D). Interestingly, in endothelial cells expressing doppel we detected reduced levels of cell surface VEGFR2 (Fig. 4E), although VEGFR2 and several intracellular signaling effectors are activated in a doppel-dependent manner (Figs 2 and 3). These data match with prior studies showing that the bulk of VEGFR2 signaling in endothelial cells occurs after ligand-induced internalization (Nakayama et al., 2013).

Functions for doppel in angiogenesis *in vivo* were next analyzed in wild-type and *Prnd*$^{-/-}$ mice, which have been described previously (Tamgüney et al., 2008). We first used a mouse hindbrain flat-mount method to quantify *Prnd*-dependent vascular morphogenesis at E12.5 (Fig. 5A). In this model, VEGF and other factors produced by hindbrain radial glial cells in the subventricular region stimulate sprouting angiogenesis from a primary vascular plexus at the pial surface (Fantin et al., 2013). In comparison with wild-type controls (n=4), defective endothelial cell sprouting into the hindbrain was obvious in *Prnd*$^{-/-}$ embryos (n=4), as revealed by abnormal patterns of blood vessel staining with AlexaFluor488-conjugated isolectinB4, which binds directly to vascular endothelial cells. Analysis of the ventricular surface of the hindbrain flat mount revealed a less elaborate vascular network, with angiogenic blood vessels displaying aberrant radial projections from the pial surface. Unlike control brains (Fig. 5B), many *Prnd*$^{-/-}$ blood vessels along the hind brain ventricular boundary showed distended and aggregated morphologies at the midline (Fig. 5C). Analysis of the pial vascular network did not reveal significant *Prnd*-dependent differences in blood vessel density, supporting the premise that the subventricular defects in *Prnd*$^{-/-}$ mice are caused by defective endothelial cell sprouting. *Prnd*$^{-/-}$ hind brain ventricular regions

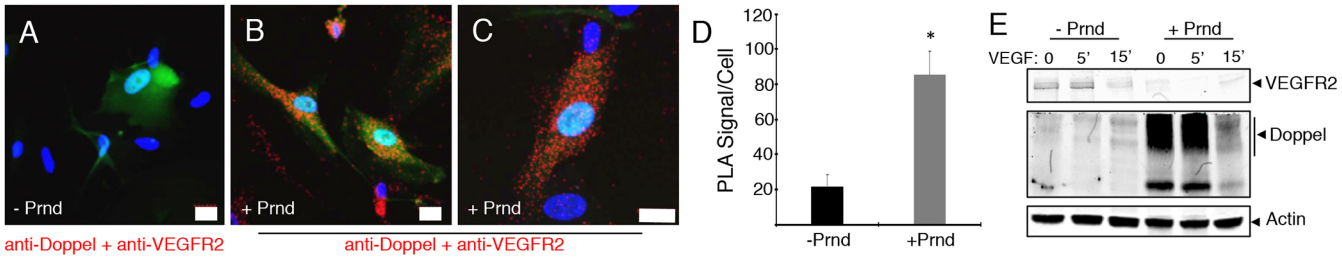

Fig. 4. Doppel interacts with VEGFR2 in brain endothelial cells. (A-C) Proximity ligation assays were performed with control HBMECs (A) or HBMECs expressing doppel (B,C), revealing direct interactions between VEGFR2 and doppel proteins. Red fluorescent signals (right panels) indicate doppel-VEGFR2 protein complexes in HBMECs. (D) Quantitation of doppel-VEGFR2 protein interactions in HBMECs based on proximity ligation assays, *P<0.001. (E) Immunoblot revealing reduced levels of VEGFR2 in HBMECs expressing doppel. Also note that VEGF treatment results in diminished levels of doppel, suggesting VEGF-induced doppel internalization and/or shedding of doppel. Scale bars: 20 µm. A two-tailed Student's t-test was used to quantify the significance of the PLA signal in HBMECs.

Development (2020) 147, dev193094. doi:10.1242/dev.193094

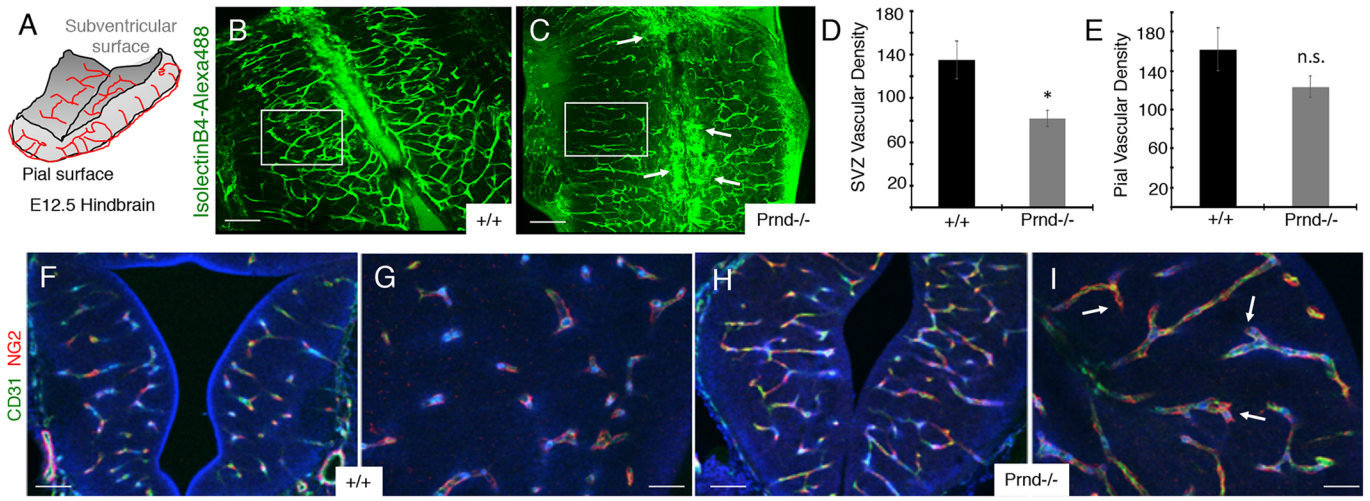

Fig. 5. Blood vessel morphogenesis defects in the *Prnd*$^{-/-}$ embryonic mouse brain. (A) Diagram of embryonic (E12.5) mouse hindbrain flat-mount showing angiogenic blood vessels (red lines) that form a primary plexus at the pial surface sprouting radially toward the ventricular region and forming more elaborate connections in neural tissue. We used this system to image and analyze blood vessel patterning in wild-type and *Prnd*$^{-/-}$ mice. This image is modified from that published by Fantin et al. (2013). (B,C) Immunofluorescence labeling of the hindbrain of E12.5 wild-type (B) or *Prnd*$^{-/-}$ embryos (C) with AlexaFluor488-conjugated isolectinB4, which labels microglia and vascular endothelial cells. Note that *Prnd*$^{-/-}$ blood vessels display distended morphologies (arrows in C). Boxed areas indicate regions used for quantitation of blood vessel densities. (D,E) Quantitation of blood vessel density based on isolectinB4:AlexaFluor488 fluorescence signal at the ventricular (D) and pial (E) regions of the hindbrain flat-mounts prepared from E12.5 wild-type and *Prnd*$^{-/-}$ embryos (n=7 brains per genotype). Note that the blood vessel densities at the pial surface are comparable between control and *Prnd*$^{-/-}$ mice (E), but there are endothelial cell sprouting defects leading to reduced blood vessel densities in the *Prnd*$^{-/-}$ subventricular zone (SVZ); *P=0.04 (D). (F-I) Immunofluorescence labeling of the midbrain of E13.5 wild-type (F,G) or *Prnd*$^{-/-}$ embryos (H,I) with anti-CD31 and anti-NG2 antibodies. Images in F and H are shown at higher magnification in G and I, respectively. Note that both wild-type control and *Prnd*$^{-/-}$ blood vessels contain vascular pericytes (arrows in I). Scale bars: 100 µm (B,C,F,H) and 50 µm (G,I). Differences among groups were analyzed using one-way ANOVA.

displayed reduced blood vessel densities (Fig. 5D), whereas the pial surface vascular network was fairly normal (Fig. 5E), further supporting roles for *Prnd* in blood vessel sprouting through the brain parenchyma. Our RTK array experiments (Fig. 3) revealed that doppel can activate phosphorylation of PDGFRβ, which shows enriched expression in vascular pericytes (Cuttler et al., 2011; Gerl et al., 2015). In addition, prior studies have reported that defective recruitment of pericytes to blood vessels causes defective angiogenesis and hemorrhage in the CNS and other organs (Gaengel et al., 2009). Although brain hemorrhage was not apparent in *Prnd*$^{-/-}$ embryos, we nonetheless analyzed whether pericyte coverage was altered in *Prnd*$^{-/-}$ brains. Coronal brain sections from wild-type (n=4; Fig. 5F,G) and *Prnd*$^{-/-}$ mice (n=4; Fig. 5H,I) revealed that blood vessels were comprised of both CD31-expressing vascular endothelial cells and NG2-expressing pericytes. There were no obvious *Prnd*-dependent differences in pericyte coverage, although *Prnd*$^{-/-}$ blood vessels displayed distended morphologies (Fig. 5H,I). Angiogenesis in the developing brain involves interactions between blood vessels and radial glial cell processes, with glial-derived growth factors and ECM cues controlling blood vessel patterning (Paredes et al., 2018). Uncoupling endothelial cell contact and communication with radial glial cells leads to severe CNS vascular pathologies. Therefore, we visualized vascular endothelial cell interactions with radial glial processes in wild-type control (n=3) and *Prnd*$^{-/-}$ (n=3) E11.5 brains by double immunofluorescence labeling with anti-CD31 and anti-nestin antibodies, respectively. Obvious *Prnd*-dependent abnormalities in the radial glial network were not detected (Fig. S6), indicating that the blood vessel morphogenesis defects in *Prnd*$^{-/-}$ embryos are probably not a secondary effect of abnormal formation of radial glial networks in the brain.

Brain angiogenesis is robust in the early postnatal period, with organ size expansion requiring a more elaborate blood vessel network to support neural cell growth, differentiation and migration. Unlike wild-type control brains (n=4; Fig. 6A,E), neonatal *Prnd*$^{-/-}$ brains (n=3; Fig. 6B,F) analyzed at P5 displayed vascular pathologies in the cerebral cortex and cerebellum, including distended tortuous blood vessels surrounded by reactive perivascular astroglial cells expressing glial fibrillary acidic protein (GFAP; Fig. 6B,F). GFAP expression is upregulated in reactive astrocytes in response to brain pathology (Liddelow and Barres, 2017); hence, it is likely that the higher GFAP expression in cerebellar astrocytes of *Prnd*$^{-/-}$ mice is a secondary result of the blood vessel abnormalities. Electron microscopy (EM)-based ultrastructural analyses of control (n=3; Fig. 6C,G) and mutant brains (n=3; Fig. 6D,H) confirmed blood vessel dilation in *Prnd*$^{-/-}$ mice. We also detected gaps between *Prnd*$^{-/-}$ vascular cells and surrounding neural cells of the parenchyma (Fig. 6D,H), unlike the control brains, which showed tight juxtaposition between neural cells and blood vessels (Fig. 6C,G).

The gaps between blood vessels and the surrounding parenchyma in *Prnd*$^{-/-}$ mice detected by EM is indicative of brain edema as a result of abnormal BBB integrity, as described in other mutant mouse models (McCarty et al., 2002; Mobley et al., 2009). Therefore, we used immunofluorescence to analyze distribution of the endogenous 69 kDa circulating biomarker, mouse serum albumin (mSA), which does not normally cross the intact BBB (LeVine, 2016). In control mice at P12 and P30 (n=3), ages when the BBB has fully formed and displays selective permeability properties for many circulating proteins, we detected mSA contained within the lumens of brain blood vessels. (Fig. 7A,C). In contrast, in *Prnd*$^{-/-}$ mice at P12 and P30 there was leakage of mSA into the parenchyma of the cerebral cortex (Fig. 7B,D). Many neuronal cell bodies showed

Development (2020) 147, dev193094. doi:10.1242/dev.193094

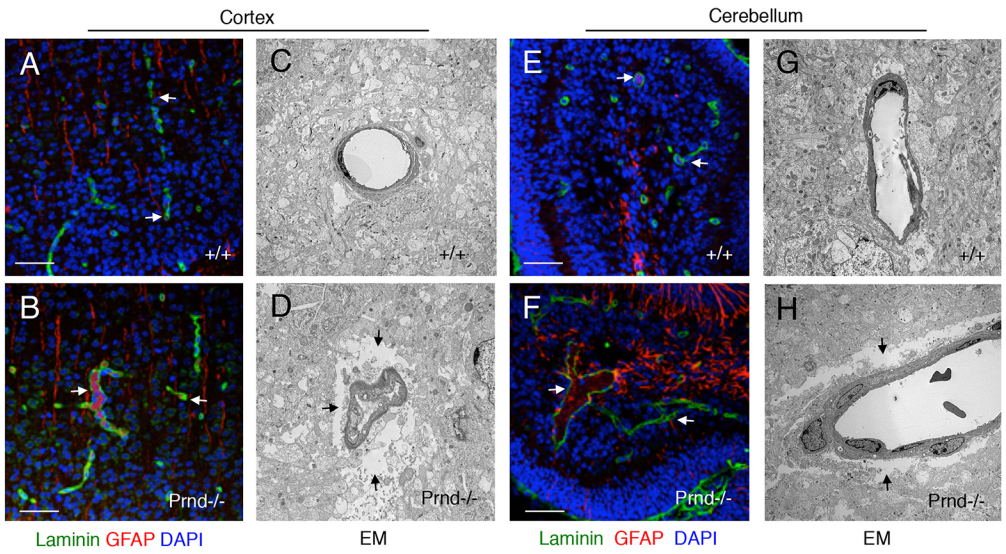

Fig. 6. Cerebrovascular pathologies in *Prnd*$^{-/-}$ neonatal mice. (A-H) Sagittal sections were prepared from P5 wild-type (A,C,E,G) or *Prnd*$^{-/-}$ mouse pups (B,D,F,H). Sections from the cerebral cortex (A,B) or cerebellum (E,F) were analyzed by immunofluorescent labeling of tissues with anti-laminin and anti-GFAP antibodies. Alternatively, regions from the cerebral cortex (C,D) or cerebellum (G,H) were analyzed at the ultrastructural level using transmission electron microscopy (C,D,G,H). In the *Prnd*$^{-/-}$ brain samples, note that the dilated blood vessels are surrounded by GFAP-expressing reactive astrocytes (arrows in B,F). *Prnd*$^{-/-}$ blood vessels also show separation from the surrounding brain parenchyma, as revealed by electron microscopy (arrows in D,H). Scale bars: 50 µm (A,B,E,F).

immunoreactivity for extravasated mSA in *Prnd*$^{-/-}$ mice. Interestingly, at P60, mSA is largely retained in the lumens of *Prnd*$^{-/-}$ blood vessels, as in wild-type control littermates (Fig. 7E,F). Quantitation of mSA levels confirmed significant leakage in the P12 and P30 *Prnd*$^{-/-}$ brains, but relatively normal luminal retention at P60 (Fig. 7G). The blood vessel morphologies in P60 adult brains were not noticeably different in control and *Prnd*$^{-/-}$ mice (Fig. 7E,F). However, to determine whether there were continued size-selective defects in the BBB of P60 *Prnd*$^{-/-}$ mice, we cardiac-perfused the 443 Da tracer NHS-biotin, which does not normally cross the BBB (Nitta et al., 2003). As shown in Fig. 7H-J, there was obvious leakage of NHS-biotin across the BBB and accumulation in the surrounding parenchyma in P60 *Prnd*$^{-/-}$ mice, but not in age-matched controls. We also detected perivascular microgliosis in the brains of P30 *Prnd*$^{-/-}$ mice (Fig. S7), which probably occurs in response to the BBB pathologies. The mSA extravasation in *Prnd*$^{-/-}$ mice detected by immunofluorescence was also obvious using immunohistochemistry methods (Fig. S8). Collectively, these data reveal that BBB abnormalities persist in adult *Prnd*$^{-/-}$ mice, although with increase in postnatal age there is some size-selective exclusion of larger macromolecules.

The mouse retina is an excellent model for studying developmental angiogenesis, because retinal vascularization occurs in a well-defined series of steps in the early neonatal period (Fruttiger, 2007). In addition, the relatively thin cytoarchitecture of the retinal tissue allows for quantitative analysis of the angiogenic vascular network, including endothelial tip cell features at the leading front of blood vessels (Hirota et al., 2015, 2011). During neonatal retinal development, a primary vascular plexus forms between P1 and P7, followed by development of a more complex secondary vascular

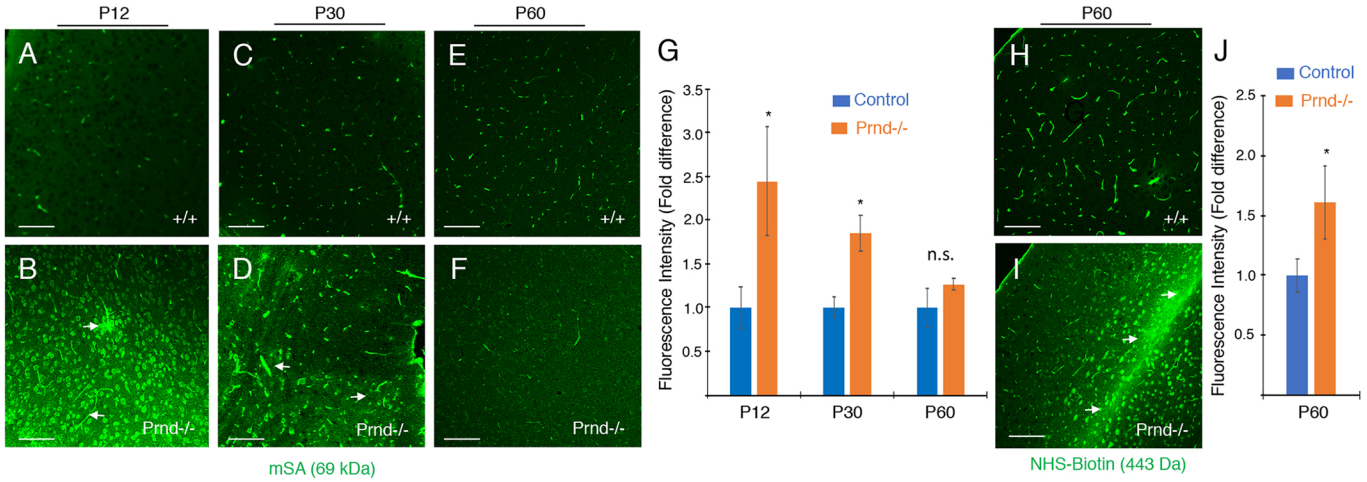

Fig. 7. Adult *Prnd*$^{-/-}$ mice display size-selective BBB defects. (A-F) Coronal brain sections from P12 (A,B), P30 (C,D) and P60 (E,F) wild-type control (A,C,E) and *Prnd*$^{-/-}$ (B,D,F) mice (n=3 mice per age and genotype) were analyzed using anti-mSA antibodies to monitor BBB integrity. Note that P12 and P30 *Prnd*$^{-/-}$ mice display obvious mSA leakage across the BBB and accumulation in the brain parenchyma (arrows in B,D), with many neuronal cell bodies showing labeling for mSA. (G) Quantitation of mSA extravasation in wild-type and *Prnd*$^{-/-}$ brains at P12, P30 and P60 based on measurement of mean immunofluorescence intensity; *P=0.02 at P12 and *P=0.03 at P30. (H,I) P60 wild-type control (H) and *Prnd*$^{-/-}$ mice (I) were cardiac-perfused with a 443 Da amine-reactive biotin (NHS-biotin) that does not normally cross the BBB. NHS-biotin distribution was analyzed in sagittal brain sections using streptavidin-AlexaFluor488. Note that control mice retain biotin in blood vessels, but adult *Prnd*$^{-/-}$ mice display focal leakage of biotin into the parenchyma (arrows in I). (J) Comparison of biotin extravasation in P60 wild-type and *Prnd*$^{-/-}$ mice (n=3 per genotype) based on quantitation of mean fluorescence intensity; *P=0.01. Differences among groups were analyzed using one-way ANOVA.

Development (2020) 147, dev193094. doi:10.1242/dev.193094

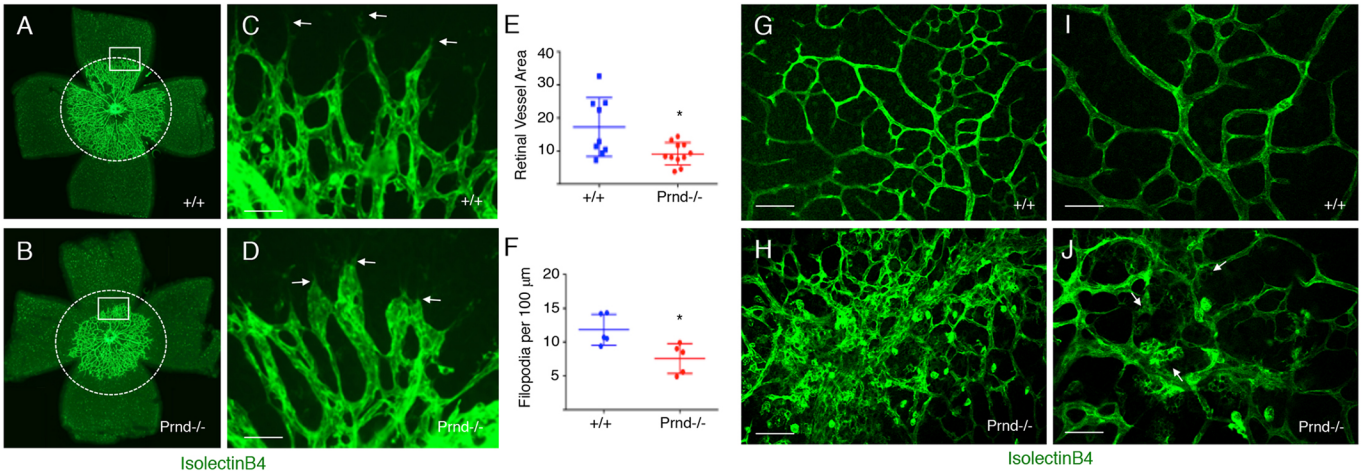

Fig. 8. Defective retinal angiogenesis in *Prnd*$^{-/-}$ neonatal mice. (A-D) P3 wild-type (A) and *Prnd*$^{-/-}$ (B) retinas were stained with isolectinB4:AlexaFluor488 to fluorescently label endothelial cells in the primary vascular plexus. Note the reduced blood vessel coverage in the *Prnd*$^{-/-}$ retinas. Dashed circles contain the same areas. Boxed areas in A and B highlighting the invading endothelial tip cell front are shown at higher magnification in C and D. Note the blunted endothelial tip cell morphologies in *Prnd*$^{-/-}$ retinas (arrows in D). (E,F) Quantitation of fluorescent (isolectinB4:AlexaFluor488-positive) area covered by the primary vascular plexus (E) and tip cell filopodia length (F) in wild-type and *Prnd*$^{-/-}$ retinas; **P*=0.02 (E), **P*=0.01 (F). (G-J) To analyze the secondary vascular plexus, retinas from P12 wild-type (G,I) and *Prnd*$^{-/-}$ (H,J) mice were dissected and labeled with isolectinB4:AlexaFluor488 to visualize blood vessels and microglia. Note the increased numbers of perivascular microglia in the *Prnd*$^{-/-}$ retina (arrows in J), probably the secondary result of vascular leakage. I and J are higher magnification images from G and H, respectively. Scale bars: 50 µm (C,D), 100 µm (G,I) and 40 µm (H,J). Unpaired two-tailed Student's *t*-test was used to determine statistically significant differences between groups.

plexus in deeper retinal layers beginning around P8. *Prnd* mRNA was enriched in retinal vascular endothelial cells, based on expression analysis in the NCBI GEO database (Fig. S9A). Anti-doppel immunohistochemistry also revealed protein expression in blood vessels of both the primary vascular plexus (Fig. S9B) and secondary vascular plexus (Fig. S9C) in developing retina. In comparison with P3 wild-type control retinas (n=3), *Prnd*$^{-/-}$ retinas (n=3) displayed impaired sprouting blood vessels in the developing primary vascular plexus. Capillary endothelial tip cells, which have low proliferation but are highly migratory, play important roles in blood vessel sprouting during retinal angiogenesis (Gerhardt et al., 2003). Quantitation of endothelial tip cell morphologies in control retinas (n=3; Fig. 8A,C) versus *Prnd*$^{-/-}$ retinas (n=3; Fig. 8B,D) revealed *Prnd*-dependent defects in sprouting angiogenesis, with *Prnd*$^{-/-}$ retina blood vessels encompassing a reduced area (Fig. 8E). Along these lines, *Prnd*$^{-/-}$ capillary endothelial tip cells appeared blunted and displayed fewer filopodia protruding into the surrounding retinal microenvironment (Fig. 8F). Development and patterning of larger arteries and veins appeared normal in *Prnd*$^{-/-}$ mice (Fig. S10). Interestingly, when we analyzed the retinal vasculature at P7, a developmental age when the primary plexus has largely formed but just prior to initiation of secondary plexus formation, angiogenesis defects were no longer obvious in *Prnd*$^{-/-}$ mice (Fig. S10). Hence, there are *Prnd*-dependent defects in retinal angiogenesis during the early stages of primary vascular plexus development (P3) that are largely restored during later stages of primary plexus formation (P7). However, analysis of the secondary vascular plexus in wild-type (Fig. 8G,I) and *Prnd*$^{-/-}$ (Fig. 8H,J) retinas at P12 (n=3 per genotype) revealed focal perivascular microgliosis in *Prnd*$^{-/-}$ mice. In addition, we detected focal intraretinal hemorrhage (data not shown) within the secondary vascular plexus of 60% of *Prnd*$^{-/-}$ mice analyzed between P10 and P14 (three out of five mice with hemorrhage), whereas no hemorrhage was detected in wild-type control retinas (n=7 mice). Collectively, these results reveal that doppel promotes angiogenesis and BBB integrity in the developing CNS via spatiotemporal activation of signaling cascades in vascular endothelial cells (Fig. 9).

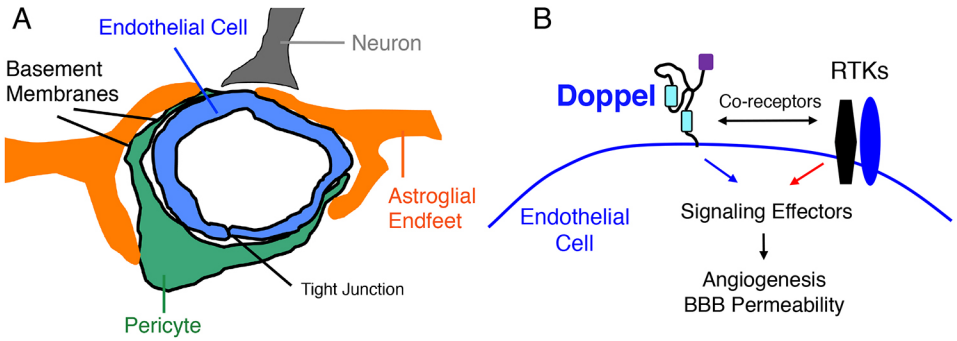

Fig. 9. Model for doppel activation of signaling pathways to promote CNS angiogenesis and endothelial barrier development. (A) Diagram showing the multicellular architecture of a brain NVU, comprising vascular endothelial cells and pericytes as well as closely juxtaposed perivascular astrocytes and neurons. Perivascular microglial cells are also components of the NVU. (B) Model for doppel regulation of CNS angiogenesis via interactions with RTKs in vascular endothelial cells. Doppel promotes RTK endocytosis, leading to activation of cytoplasmic enzymatic pathways and gene regulatory networks. These events collectively promote angiogenesis and BBB formation in the developing CNS.

Development (2020) 147, dev193094. doi:10.1242/dev.193094

DISCUSSION

Our various *in vitro* and *in vivo* data reveal that (i) doppel is expressed exclusively in angiogenic vascular endothelial cells in the developing mouse brain and retina but is reduced in quiescent endothelial cells in the adult CNS (Fig. 1); (ii) GPI-linked doppel activates cytoplasmic signaling pathways in endothelial cells via interactions with transmembrane RTKs, including the VEGF-A receptor VEGFR2 (Figs 2-4); and (iii) *Prnd*$^{-/-}$ mice display defects in sprouting angiogenesis in the developing brain and retina, as well as impaired CNS barrier integrity (Figs 5-8). A previous study has shown that the bulk of VEGFR2 signaling *in vivo* occurs after internalization, with precise regulation of VEGFR2 cell surface levels promoting endothelial tip cell polarity and sprouting functions at the invading front of angiogenic blood vessels (Pitulescu and Adams, 2014). We propose that doppel plays a key regulatory role in promoting VEGFR2 internalization to promote intracellular signaling in endothelial cells (Fig. 9). A prior study in HUVECs revealed that VEGFR2 endocytosis occurs in the absence of ligand stimulation (constitutive internalization) via clathrin-mediated endocytosis and involves the clathrin adaptor protein Dab2 as well as the polarity factor Par-3 (Nakayama et al., 2013). In contrast, ligand-induced VEGR2 internalization occurs through the formation of large endocytic vesicles via Cdc42-dependent mechanisms (Basagiannis et al., 2016). Doppel in tumor endothelial cells also promotes VEGFR2 internalization (Al-Hilal et al., 2016). Although our data reveal that doppel in the brain vascular endothelium stimulates VEGFR2 signaling in a ligand-independent manner and probably involves clathrin-mediated endocytosis, more experiments are necessary to determine whether doppel also has a role in ligand-induced VEGFR2 internalization and signaling and whether there is cross-talk between doppel and signaling effectors such as Par-3. Interestingly, we detected a rapid VEGF-induced reduction in doppel levels in brain endothelial cells, suggesting that VEGF stimulates the membrane release of GPI-linked doppel. A prior report has shown that VEGF stimulation of endothelial cells activates the proteolytic activity of disintegrin and metalloprotease 10 (ADAM10), leading to proteolysis and membrane release of neuropilin-1 (Mehta et al., 2018). ADAM10 is a broadly expressed 'sheddase' that also mediates cleavage of Prp^{c} from the surface of neurons (Linsenmeier et al., 2017). It will be interesting to determine whether ADAM10 and/or other proteases mediate release of doppel from the endothelial cell surface. In addition to *cis* interactions with VEGFR2 in endothelial cells, we have found links between doppel and other RTKs, including PDGFRβ, which is expressed primarily in vascular pericytes. Although we did not detect defects in pericyte coverage of blood vessels in *Prnd*$^{-/-}$ mice, it will be interesting to determine whether doppel regulates PDGFRβ signaling functions via intercellular interactions between endothelial cells and pericytes and how these potential *trans* binding events impact blood vessel morphogenesis.

Expression of *Prnd* RNA and doppel protein in mouse brain endothelial cells is greatly diminished beginning at ∼P7 and is absent in the adult brain. This downregulation of *Prnd* correlates with endothelial cell differentiation and the onset of blood vessel quiescence (Tam and Watts, 2010). In addition, endogenous *Prnd* mRNA and doppel protein were not detected in any endothelial cell type analyzed. Activation of pathological angiogenesis during malignant human brain tumor growth leads to increased doppel expression in sprouting blood vessels. Collectively, these data suggest that cues within the brain microenvironment control *Prnd* expression to promote angiogenesis. It is important to determine the identities of these cues and probe their molecular mechanisms of action. Doppel is also expressed in the vascular endothelial cells outside of the CNS. For example, in the developing intestinal tract we detected robust doppel expression in capillaries of the newly formed epithelial villi. Whether doppel is necessary for normal intestinal vascularization via control of RTK signaling or other pathways remains to be explored. In addition, the testes display the highest levels of doppel expression (Qin et al., 2013), primarily within Sertoli cells of seminiferous tubules, which are involved in sperm production. There are several growth factors and hormonal cues that promote spermatogenesis, raising the intriguing possibility that sterility in *Prnd*$^{-/-}$ male mice is caused by defective doppel control of intracellular signaling cascades, possibly involving RTKs or other transmembrane receptors.

Given that *Prnd* mRNA expression in brain endothelial cells was first reported 20 years ago (Li et al., 2000) and ablation of the *Prnd* gene in mice was published nearly 12 years ago (Tamgüney et al., 2008), it is somewhat surprising that *Prnd*-dependent developmental vascular pathologies have not been reported prior to this publication. One reason may be that the sprouting angiogenesis pathologies we have detected in the *Prnd*$^{-/-}$ mouse brain and retina are subtle, especially compared with phenotypes in other mutant mouse models that develop more severe brain vascular phenotypes (McCarty, 2020). However, the BBB pathologies in the neonatal developmental period are quite obvious, with focal extravasation of the relatively large 69 kDa mSA protein and accumulation in the brain parenchyma of *Prnd*$^{-/-}$ mice. The focal nature of BBB leakage probably reflects the heterogeneous expression of doppel detected by us in brain endothelial cells, with many blood vessels lacking expression and others expressing robust levels of doppel. Interestingly, the BBB defects in *Prnd*$^{-/-}$ mice become normalized with age and, at P60 we detect relatively normal exclusion of mSA, although small molecule tracers are able to extravasate. This partial 'repair' in BBB integrity coincides, in part, with diminished *Prnd* expression in quiescent brain endothelial cells. Adult *Prnd*$^{-/-}$ mice do not display obvious neurological phenotypes and survive for more than a year, comparable to wild-type littermates. We propose that *Prnd* regulates signaling pathways and gene expression events that collectively contribute to BBB formation during development, with these processes downregulated in the healthy adult brain. It will be interesting to manipulate *Prnd* expression temporally in adult brain endothelial cells to determine whether acute loss of expression or inducible activation of expression impacts angiogenesis and BBB physiology.

MATERIALS AND METHODS

Experimental mice and genotyping

All mouse experiments were reviewed and approved prior to animal use under the guidance of the Institutional Animal Care and Use Committee (IACUC) and the MD Anderson Subcommittee on Animal Studies, both AAALAC accredited institutions. Generation of *Prnd*$^{+/-}$ mice has been described previously (Tamgüney et al., 2008). DNA was extracted by proteinase K digestion of ear snip tissue, followed by ethanol precipitation and DNA resuspension. Alleles were identified by PCR using DNA (50 ng), MangoMix Taq DNA Polymerase (Meridian, Memphis, TN) and primers (1 µM). *Prnd* wild-type and null alleles were discerned by a two primer PCR. Reactions (50 µl) were run using primers *Prnd* forward 5′-CGATG-CAACGAGTGATGAGGTTCGC-3′ and reverse 5′-GCTAACCAGCGT-TTTCGTTCTGCC-3′, under the following PCR conditions: initial 94°C for 2 min, 35 cycles of 94°C for 15 s, 68°C for 15 s and 72°C for 2 min, final 72°C for 10 min followed by holding the samples at 4°C. The *Prnd* primers sit outside of the *Prnd* open reading frame and yield a 1.5 kb band for the wild-type allele and 1.0 kbp band for the shorter *Prnd* null locus allele.

RNA extraction and qRT-PCR

Freshly isolated mouse brains (n=3 per age and genotype) were snap frozen and the total RNA extracted following the Qiagen RNeasy microkit guidelines. RNA was reverse transcribed using Invitrogen SuperScript III

Development (2020) 147, dev193094. doi:10.1242/dev.193094

cDNA synthesis kit, and 100 ng cDNA was used per reaction. Quantitative RT-PCR to analyze *Prnd* expression in mouse brain tissue was performed using a StepOnePlus Real-Time PCR system (Applied Biosystems). The following primers were used: murine *Prnd* forward 5′-AGGGGCATAA-AGCACAGGTT-3′ and reverse 5′-ATCTCCTTGGTCACGTTGGC-3′ and murine *Gapdh* forward 5′-AGGTCGGTGTGAACGGATTTG-3′ and reverse 5′-GGGGTCGTTGATGGCAACA-3′. Levels of *Prnd* RNA were standardized based on GAPDH expression levels. All PCR reactions were performed in triplicate.

Isolation of CD31$^+$ primary mouse brain endothelial cells

Mouse pups were euthanized by CO_2 in accordance with IACUC regulations. Mouse brains were dissected, manually dissociated and CD31-positive cells selected using the Miltenyi Biotec Adult Brain Dissociation Kit (130-107-677), CD31 Microbeads (130-097-418) and LS Columns (130-042-401). Briefly, the brains were minced, enzymatically digested and homogenized by means of gentle trituration. The brain homogenate was filtered through a 70 µm cell strainer to obtain a single cell suspension. Debris and myelin were removed by phase separation using the debris removal solution contained in the kit. Red blood cells were removed by lysis using the red blood cell removal solution. The remaining cells were positive selected for expressing mouse CD31 antigen by labeling with Miltenyi Biotec CD31 Microbeads and then magnetically separated with Miltenyi Biotec LS Columns. The final eluted CD31-positive cell fraction was washed twice in PBS and either flash frozen on dry ice or cultured on laminin-coated plates in DMEM-F12 medium supplemented with 5% FBS, 1% ECGS and penicillin-streptomycin.

Tissue sectioning, immunofluorescence and immunoblotting

Pregnant mice were euthanized by CO_2 as per IACUC regulations. Dissection of the E12.5 wild-type and *Prnd*$^{-/-}$ embryonic hindbrains were performed as previously reported (Fantin et al., 2013). Briefly, the embryos within yolk sacs were removed from the uterus with forceps. The head was removed from the body and positioned in a convenient orientation to obtain the hindbrain with surrounding mesenchymal tissue. Using forceps, the roof plate was cut to expose the hindbrain. Pial membranes and surrounding mesenchyme were teased away from the neural tissue. Midbrain and spinal cord tissues were removed with forceps to obtain the unfurled hindbrain. Hindbrains were washed in cold PBS, fixed in cold 4% paraformaldehyde (PFA) for 2 h and stained with isolectinB4: AlexaFluor488 at 1:500 dilution in PBS containing 0.05% Triton X-100 at 4°C overnight. The sections were washed with PBS, stained with DAPI and mounted for imaging. To preserve postnatal brain cytoarchitecture, mice were cardiac-perfused with PBS containing 4% PFA. Brains were then removed from the skull and post-fixed in PBS containing 4% PFA for 16-24 h at 4°C. Following fixation, the brains were washed in PBS, cut sagitally or coronally and then embedded in 3% low-melt agarose for postnatal brains or 4% low-melt agarose for embryonic brains. The agarose block was trimmed and attached to the vibratome specimen disc within the buffer tray. The buffer tray was then filled with cold PBS and the block sectioned at 100 µm thickness on a Leica VT1000S vibratome. The sections were stored in PBS at 4°C until immunofluorescence staining. Free-floating 100 µm thick brain sections were blocked and permeabilized for 2 h in 10% serum (obtained from the same species as the secondary) diluted in PBS containing 0.5% Triton X-100. Sections were incubated overnight at 4°C in the primary antibody diluted in the blocking and permeabilization buffer. The sections were washed three times, each for 1 h in PBS containing 0.5% Triton X-100. Sections were incubated for 2 h in a fluorescence-labeled secondary antibody, with select affinity to the primary antibody, diluted in the blocking and permeabilization buffer. The sections were again washed three times, followed by a final PBS rinse and the mounting of sections on slides in Vectashield mounting medium with DAPI (Vector Labs). The staining was imaged using an Olympus FV1000. Immunohistochemistry was performed on formalin-fixed paraffin-embedded (FFPE) tissue according to standard protocols. The following antibodies and dilutions were used for immunofluorescence: anti-GFAP (DAKO rabbit Z0334, 1:500), anti-GFAP (Millipore mouse MAB3402, 1:200), anti-Iba1 (Wako Chemicals rabbit 01919741, 1:250), anti-NG2 (Millipore rabbit ab5320MI, 1:250), anti-CD31 (BD Biosciences rat 553370, 1:200), and anti-laminin (Sigma rat L9393, 1:50), and anti-mouse serum albumin (Mybiosource rabbit mbs2001910, 1:200). Secondary antibodies used were AlexaFluor488-conjugated affinity purified anti-rabbit, anti-mouse, anti-rat, anti-chicken and anti-goat antibodies (Jackson Labs). IsolectinB4 (Invitrogen I21411, 1:500) was also used to stain vascular endothelial cells.

The following commercially available antibodies were used for immunoblotting: anti-PY99 (Santa Cruz sc-7020, 1:1000), anti-phospho-VEGFR2 pY1214 (R&D cat#AF1766, 1:800), anti-phospho-PDGFRα/β pY1021 (R&D cat#AF2316, 1:1000), anti-phospho-MSPR/Ron pY1238/123 (R&D cat#AF1947, 1:1000) and anti-actin AC-15 (Abcam #ab6276, 1:5000). The following antibodies were purchased from Cell Signaling Technologies: anti-phospho-Met pY1234/1235 (#3044 1:1000), anti-phospho-Akt pS473 (#4060, 1:2000), anti-Akt (#9272, 1:1000), anti-Erk1/2 (#9107, 1:1000), anti-phospho-Erk1/2 pT202/pT204 (#9106, 1:2000), anti-VEGFR2 (#2479L, 1:1000) and anti-phospho-VEGFR2 pY1175 (CST2478, 1:1000). Immunoblots were overlaid with donkey anti-rabbit 800, donkey anti-mouse 680, and donkey anti-goat 800 secondary antibodies purchased from Licor (1:15,000). Antibodies were added in blocking buffer comprising 3% bovine serum albumin (BSA) in Tris-buffered saline containing 0.1% Tween-20.

Human brain endothelial cell experiments

Primary HBMECs were purchased from ScienCell Research Laboratories (cat#1000), and were maintained in endothelial cell medium (ECM, cat#1001). HBEC-5i cells were purchased from the ATCC (CRL-3245) and maintained in DMEM-F12 medium containing 10% FBS, endothelial cell growth supplement (ECGS, Cat #1052), and 1% penicillin-streptomycin antibiotic solution. Cells were grown on dishes coated with rat tail collagen (Sigma-Aldrich) at 37°C and 5% CO_2. For lentivirus infections, HBMECs were seeded into six-well plates at a concentration of 5×10^5 cells/well and cultured in complete medium for 24 h. Cells were infected with pLOC lentivirus expressing human PRND and GFP (PLOHS-100071420) or with lentivirus-mediated pLOC negative control (GFP/RFP). After 48 h, 5 µg/ml of blasticidin-S hydrochloride (Sigma, #15205) was added to cells. Drug selection occurred for 5-7 days and then cells were FAC sorted based on expression of GFP. PRND-dependent cell viability was quantified by counting adherent cells grown in complete medium using the Celltiter-Glo luminescent cell viability assay kit according to the manufacturer's protocol. Briefly, cells were collected and 5×10^3 cells were plated into 96-well plates. Celltiter-Glo reagent was added in culture medium to each well. Plates were incubated at room temperature for 10 min and the luminescence intensity measured with a microplate reader. Matrigel chambers were purchased from Corning (354480). The upper chamber was seeded with 5×10^4 HBMECs in DMEM Ham's F12 medium with 0.1% fetal bovine serum. The lower chamber was filled with DMEM Ham's F12 medium containing only 10% fetal bovine serum as a chemoattractant. All media contained 1× penicillin-streptomycin. Cells were incubated at 37°C with 5% CO_2 for 24 h. Non-invading cells were removed by vigorous cotton swabbing. The remaining cells on the filters were fixed in 4% PFA and stained with hematoxylin followed by quantitation of invasion. For VEGF stimulation, subconfluent cultures of HBMECs were serum starved overnight. Cells were then treated with 50 ng/ml recombinant human $VEGF_{165}$ (Biolegend cat#583704) in basal DMEM/F-12 (1:1) medium without FBS. After the medium was removed, cells were washed twice in ice-cold PBS. The cell lysate was prepared using RIPA lysis buffer.

Phospho-RTK antibody arrays

Phosphorylation of RTKs in HBMECs was analyzed by the Proteome Profiler Array Kit (Human-phospho-RTK array) (R&D Systems, # ARY001B) and was used to determine the relative levels of tyrosine phosphorylation of 49 different RTKs according to the manufacturer's protocol. Briefly, membranes with duplicate antibody spots were blocked and incubated with 200-300 µg HBMEC (with or without Prnd) lysates overnight at 4°C. Membranes were then washed in buffer and incubated with the secondary antibody (HRP-conjugated anti-phosphotyrosine) for 2 h at room temperature. Membranes were washed before development with ECL immunoblotting detection reagent (GE Healthcare). Spots of different RTKs were visualized using the ECL chemiluminescence detection system

Development (2020) 147, dev193094. doi:10.1242/dev.193094

(GE Healthcare). Pixel densities on developed X-ray film were collected using a transmission mode scanner and quantified using ImageJ software (National Institutes of Health).

Doppel antibody generation

Anti-doppel polyclonal rabbit polyclonal antibodies were generated using a synthetic 20-residue peptide sequence corresponding to amino acids 55-73 (RPGAFIKQGRKLDIDFGAEC) of the human doppel protein. This sequence is 100% identical to the mouse doppel protein, as determined by sequence alignment using BLAST. Pre-bleeds were taken from two rabbits in parallel with synthesis of the selected peptide conjugated to the immunogenic KLH carrier protein. Six weeks later, the rabbits were immunized by subcutaneous injection with the KLH conjugated peptide. After 10 days, the first production bleed was taken from each rabbit. At 10 days after the bleed, the rabbits were delivered a second booster immunization. After another 10 days, the rabbits were bled a second time. Antibody specificities from each bleed were tested by ELISA, immunoblotting and immunohistochemistry. Promising bleeds were affinity purified using the immunizing peptide.

Reverse phase protein arrays

Adherent cells were washed twice in ice-cold PBS, then lysed in RIPA buffer or RPPA lysis buffer containing 1% Triton X-100, 50 mM HEPES pH 7.4, 150 mM NaCl, 1.5 mM $MgCl_2$, 1 mM EGTA, 100 mM NaF, 10 mM sodium pyruvate, 1 mM Na_3VO_4, 10% glycerol and a cocktail of protease and phosphatase inhibitors (Roche Diagnostics, Mannheim, Germany) for 20-30 min with frequent mixing on ice. Samples were then centrifuged at 11,000 ***g*** at 4°C for 15 min to isolate the detergent-soluble protein supernatant. Protein concentration was determined using the BCA assay (or Bradford); the optimal protein concentration of lysates for RPPA was about 1.2 µg/µl (1.2 mg/ml). Lysates were denatured in 4× SDS/2-ME sample buffer (35% glycerol, 8% SDS, 0.25 M Tris-HCl pH 6.8 and no β-mercaptoethanol) for 5 min at 95°C. Lysates were stored at −80°C and subsequently analyzed in the RPPA core facility at MD Anderson Cancer Center (University of Texas). Samples were serially diluted and probed with 447 antibodies and arrayed on nitrocellulose-coated slides. Relative protein levels were normalized for protein loading and determined by interpolation of each dilution curve from the standard curve. Normalized data points were transformed to a linear value used for analysis.

Proximity ligation assays

The Duolink In Situ Red Starter Kit (Sigma-Aldrich) was used to analyze interactions between VEGFR2 and doppel in HBMEC cells. Briefly, HBMECs were cultured on eight-chamber polystyrene culture slides (Falcon, NY, USA) overnight. Slides were washed twice with PBS, fixed with 4% PFA for 15 min and permeabilized with PBS containing 0.1% Triton X-100 for 10 min. After two PBS washes, the cells were incubated with blocking solution for 1 h and then with the primary mouse anti-human VEGFR2 and rabbit anti-human PRND antibodies overnight at 4°C. Samples were then washed twice for 5 min with buffer A, followed by incubation with the PLA probes (secondary antibodies against two different species bound to two oligonucleotides: anti-mouse MINUS and anti-rabbit PLUS) in antibody diluent for 60 min at 37°C. After two washes of 5 min with buffer A, the ligation step was performed with ligase diluted in ligation stock for 30 min at 37°C. In the ligation step, the two oligonucleotides in the PLA probes were hybridized to the circularization oligonucleotides. The cells were washed twice with buffer A for 5 min and incubated for 100 min with amplification stock solution at 37°C. The amplification stock solution contains polymerase for the rolling circle amplification step and oligonucleotides labeled with fluorophores, which bind to the product of the rolling circle amplification and thus allow detection. After two washes of 10 min with buffer B, cells were mounted with Duolink *in situ* mounting medium containing DAPI. For every antibody, a negative control experiment was performed where only one antibody was incubated with the PLA probes. PLA signals (red fluorescent spots), each representing a close proximity of these two targets, were examined using a confocal laser scanning microscope and quantified with ImageJ. The mean fluorescence intensity of the PLA signal per cell was quantified. The data were collected from 40 images of HBMEC cells using GraphPad Prism. A two-tailed Student's *t*-test was used to quantify the significance of the PLA signal in HBMECs.

Biotin perfusions and BBB analyses

P60 control and mutant animals were deeply anesthetized and a 20 G needle was inserted into the left ventricle of the heart. Animals were first perfused with 20 ml of PBS to flush the circulation so that no residual cells or serum proteins were labeled with reactive biotin. Animals were then perfused for 5 min continuously with 1 mg/ml EZLink-NHS-Biotin (Pierce Chemicals) dissolved in PBS (approximately 7.5 ml in total per animal). Animals were then perfused with 4% PFA in PBS as fixative to preserve brain morphology. Sagittal or coronal brain sections were prepared with a vibratome or brains were embedded in paraffin and sectioned. Brain sections were labeled with streptavidin-AlexaFluor488 (Molecular Probes) to visualize biotin distribution. ImageJ software was used for quantitation of biotin extravasation (n=3 wild-type and $Prnd^{-/-}$ mice) using randomly selected 20× images (n=3 per sample) taken from the cerebral cortex. ImageJ software was also used to quantify mouse serum albumin extravasation in P60 wild-type and $Prnd^{-/-}$ mice (n=3 per genotype) using 20× fluorescence images (n=3-5 per genotype) taken from the cerebral cortex.

Whole-mount retinal analysis

Wild-type (n=5) or $Prnd^{-/-}$ neonatal mice (n=3) were sacrificed and eyes were removed and fixed in 4% PFA in PBS at 4°C for 4 h. Whole retinal cups were then microdissected, blocked in 1% BSA with 0.1% Triton X-100 in PBS and incubated with primary antibodies for 16 h at 4°C. Tissues were then washed five times in PBS at room temperature and incubated overnight with secondary antibodies. Washed retinal cups were then flat-mounted on microscope slides. For quantitation of retinal defects to quantify numbers of filopodia per tip cell, randomly selected micrograph images (n=3 images per retina, n=3 mice per genotype) were analyzed at 400× magnification. Individual tip cells (>25 cells per genotype) were identified at the leading edge of the retinal vascular front, and filopodia stained with IsoB4-AlexaFluor488 were counted. Alternatively, to quantify filopodia sprouts per vessel length, ImageJ software was used to count filopodia projections per 100 µm at the leading edge of the migrating vessel front (n=3 images per retina, n=3 mice per genotype). Student's *t*-test was performed to determine statistically significant differences between groups.

Statistical analysis

All data herein represent replicates of three or more and are presented as the mean±s.d., unless otherwise indicated. Differences among groups were analyzed using one-way ANOVA or unpaired two-tailed Student's *t*-test. When overall analysis revealed significance among groups, means were compared and tested using Tukey post hoc analysis. Statistical significance was set at $P<0.05$. All statistical analyses were performed using Graphpad Prism 8 or SigmaPlot 12.0 software (Systat Software).

Acknowledgements

We are grateful to Dr Stanley Prusiner and members of his group (UCSF) for providing the frozen sperm used for rederivation of the $Prnd^{+/-}$ mice. In addition, we thank the members of the McCarty laboratory for insightful comments on the manuscript.

Competing interests

The authors declare no competing or financial interests.

Author contributions

Conceptualization: J.H.M.; Methodology: Z.C., J.E.M., N.A., P.A.G., J.H.S.; Formal analysis: Z.C., N.A.; Investigation: Z.C., J.E.M., N.A., P.A.G., J.H.S., J.H.M.; Resources: G.R.; Writing - original draft: J.H.M.; Writing - review & editing: Z.C., J.E.M., N.A., P.A.G., J.H.M.; Supervision: J.H.M.; Project administration: J.H.M.; Funding acquisition: J.H.M.

Funding

This work was supported, in part, by grants to J.H.M. from the Cancer Prevention and Research Institute of Texas (RP180220) and the National Institutes of Health (R01NS087635 and R21NS103841). Deposited in PMC for release after 12 months.

Supplementary information

Supplementary information available online at
https://dev.biologists.org/lookup/doi/10.1242/dev.193094.supplemental

References

Al-Hilal, T. A., Chung, S. W., Choi, J. U., Alam, F., Park, J., Kim, S. W., Kim, S. Y., Ahsan, F., Kim, I.-S. and Byun, Y. (2016). Targeting prion-like protein doppel selectively suppresses tumor angiogenesis. *J. Clin. Invest.* **126**, 1251-1266. doi:10.1172/JCI83427

Arnold, T. D., Niaudet, C., Pang, M.-F., Siegenthaler, J., Gaengel, K., Jung, B., Ferrero, G. M., Mukouyama, Y.-S., Fuxe, J., Akhurst, R. et al. (2014). Excessive vascular sprouting underlies cerebral hemorrhage in mice lacking alphaVbeta8-TGFbeta signaling in the brain. *Development* **141**, 4489-4499. doi:10.1242/dev.107193

Basagiannis, D., Zografou, S., Murphy, C., Fotsis, T., Morbidelli, L., Ziche, M., Bleck, C., Mercer, J. and Christoforidis, S. (2016). VEGF induces signalling and angiogenesis by directing VEGFR2 internalisation through macropinocytosis. *J. Cell Sci.* **143**, e1.1. doi:10.1242/dev.146456

Brouwer, A. J., Groenendaal, F., Benders, M. J. N. L. and de Vries, L. S. (2014). Early and late complications of germinal matrix-intraventricular haemorrhage in the preterm infant: what is new? *Neonatology* **106**, 296-303. doi:10.1159/000365127

Ciric, D. and Rezaei, H. (2015). Biochemical insight into the prion protein family. *Front. Cell Dev. Biol.* **3**, 5. doi:10.3389/fcell.2015.00005

Cuttler, A. S., LeClair, R. J., Stohn, J. P., Wang, Q., Sorenson, C. M., Liaw, L. and Lindner, V. (2011). Characterization of Pdgfrb-Cre transgenic mice reveals reduction of ROSA26 reporter activity in remodeling arteries. *Genesis* **49**, 673-680. doi:10.1002/dvg.20769

Daneman, R., Zhou, L., Kebede, A. A. and Barres, B. A. (2010). Pericytes are required for blood-brain barrier integrity during embryogenesis. *Nature* **468**, 562-566. doi:10.1038/nature09513

Didonna, A. (2013). Prion protein and its role in signal transduction. *Cell. Mol. Biol. Lett.* **18**, 209-230. doi:10.2478/s11658-013-0085-0

Fantin, A., Vieira, J. M., Plein, A., Maden, C. H. and Ruhrberg, C. (2013). The embryonic mouse hindbrain as a qualitative and quantitative model for studying the molecular and cellular mechanisms of angiogenesis. *Nat. Protoc.* **8**, 418-429. doi:10.1038/nprot.2013.015

Fruttiger, M. (2007). Development of the retinal vasculature. *Angiogenesis* **10**, 77-88. doi:10.1007/s10456-007-9065-1

Gaengel, K., Genové, G., Armulik, A. and Betsholtz, C. (2009). Endothelial-mural cell signaling in vascular development and angiogenesis. *Arterioscler. Thromb. Vasc. Biol.* **29**, 630-638. doi:10.1161/ATVBAHA.107.161521

Genet, G., Boyé, K., Mathivet, T., Ola, R., Zhang, F., Dubrac, A., Li, J., Genet, N., Henrique Geraldo, L., Benedetti, L. et al. (2019). Endophilin-A2 dependent VEGFR2 endocytosis promotes sprouting angiogenesis. *Nat. Commun.* **10**, 2350. doi:10.1038/s41467-019-10359-x

Gerhardt, H., Golding, M., Fruttiger, M., Ruhrberg, C., Lundkvist, A., Abramsson, A., Jeltsch, M., Mitchell, C., Alitalo, K., Shima, D. et al. (2003). VEGF guides angiogenic sprouting utilizing endothelial tip cell filopodia. *J. Cell Biol.* **161**, 1163-1177. doi:10.1083/jcb.200302047

Gerl, K., Miquerol, L., Todorov, V. T., Hugo, C. P. M., Adams, R. H., Kurtz, A. and Kurt, B. (2015). Inducible glomerular erythropoietin production in the adult kidney. *Kidney Int.* **88**, 1345-1355. doi:10.1038/ki.2015.274

Haynes, R. L., Sleeper, L. A., Volpe, J. J. and Kinney, H. C. (2013). Neuropathologic studies of the encephalopathy of prematurity in the late preterm infant. *Clin. Perinatol.* **40**, 707-722. doi:10.1016/j.clp.2013.07.003

Hirota, S., Liu, Q., Lee, H. S., Hossain, M. G., Lacy-Hulbert, A. and McCarty, J. H. (2011). The astrocyte-expressed integrin alphavbeta8 governs blood vessel sprouting in the developing retina. *Development* **138**, 5157-5166. doi:10.1242/dev.069153

Hirota, S., Clements, T. P., Tang, L. K., Morales, J. E., Lee, H. S., Oh, S. P., Rivera, G. M., Wagner, D. S. and McCarty, J. H. (2015). Neuropilin 1 balances beta8 integrin-activated TGFbeta signaling to control sprouting angiogenesis in the brain. *Development* **142**, 4363-4373. doi:10.1242/dev.113746

Jakobsson, L., Bentley, K. and Gerhardt, H. (2009). VEGFRs and Notch: a dynamic collaboration in vascular patterning. *Biochem. Soc. Trans.* **37**, 1233-1236. doi:10.1042/BST0371233

Jensen, L. D., Hot, B., Ramsköld, D., Germano, R. F. V., Yokota, C., Giatrellis, S., Lauschke, V. M., Hubmacher, D., Li, M. X., Hupe, M. et al. (2019). Disruption of the extracellular matrix progressively impairs central nervous system vascular maturation downstream of beta-catenin signaling. *Arterioscler. Thromb. Vasc. Biol.* **39**, 1432-1447. doi:10.1161/ATVBAHA.119.312388

Kuhnert, F., Mancuso, M. R., Shamloo, A., Wang, H.-T., Choksi, V., Florek, M., Su, H., Fruttiger, M., Young, W. L., Heilshorn, S. C. et al. (2010). Essential regulation of CNS angiogenesis by the orphan G protein-coupled receptor GPR124. *Science* **330**, 985-989. doi:10.1126/science.1196554

Lathia, J. D., Mack, S. C., Mulkearns-Hubert, E. E., Valentim, C. L. and Rich, J. N. (2015). Cancer stem cells in glioblastoma. *Genes Dev.* **29**, 1203-1217. doi:10.1101/gad.261982.115

LeVine, S. M. (2016). Albumin and multiple sclerosis. *BMC Neurol.* **16**, 47. doi:10.1186/s12883-016-0564-9

Li, A., Sakaguchi, S., Shigematsu, K., Atarashi, R., Roy, B. C., Nakaoke, R., Arima, K., Okimura, N., Kopacek, J. and Katamine, S. (2000). Physiological expression of the gene for PrP-like protein, PrPLP/Dpl, by brain endothelial cells and its ectopic expression in neurons of PrP-deficient mice ataxic due to Purkinje cell degeneration. *Am. J. Pathol.* **157**, 1447-1452. doi:10.1016/S0002-9440(10)64782-7

Liddelow, S. A. and Barres, B. A. (2017). Reactive astrocytes: production, function, and therapeutic potential. *Immunity* **46**, 957-967. doi:10.1016/j.immuni.2017.06.006

Liebner, S., Corada, M., Bangsow, T., Babbage, J., Taddei, A., Czupalla, C. J., Reis, M., Felici, A., Wolburg, H., Fruttiger, M. et al. (2008). Wnt/beta-catenin signaling controls development of the blood-brain barrier. *J. Cell Biol.* **183**, 409-417. doi:10.1083/jcb.200806024

Linsenmeier, L., Altmeppen, H. C., Wetzel, S., Mohammadi, B., Saftig, P. and Glatzel, M. (2017). Diverse functions of the prion protein - does proteolytic processing hold the key? *Biochim. Biophys. Acta Mol. Cell Res.* **1864**, 2128-2137. doi:10.1016/j.bbamcr.2017.06.022

Lührs, T., Riek, R., Güntert, P. and Wüthrich, K. (2003). NMR structure of the human doppel protein. *J. Mol. Biol.* **326**, 1549-1557. doi:10.1016/S0022-2836(02)01471-7

Ma, S., Santhosh, D., Kumar, T. P. and Huang, Z. (2017). A brain-region-specific neural pathway regulating germinal matrix angiogenesis. *Dev. Cell* **41**, 366-381.e4. doi:10.1016/j.devcel.2017.04.014

Mastrangelo, P. and Westaway, D. (2001). The prion gene complex encoding PrP(C) and Doppel: insights from mutational analysis. *Gene* **275**, 1-18. doi:10.1016/S0378-1119(01)00627-8

McCarty, J. H. (2020). alphavbeta8 integrin adhesion and signaling pathways in development, physiology and disease. *J. Cell Sci.* **133**, jcs239434. doi:10.1242/jcs.239434

McCarty, J. H., Monahan-Earley, R. A., Brown, L. F., Keller, M., Gerhardt, H., Rubin, K., Shani, M., Dvorak, H. F., Wolburg, H., Bader, B. L. et al. (2002). Defective associations between blood vessels and brain parenchyma lead to cerebral hemorrhage in mice lacking alphav integrins. *Mol. Cell. Biol.* **22**, 7667-7677. doi:10.1128/MCB.22.21.7667-7677.2002

Mehta, V., Fields, L., Evans, I. M., Yamaji, M., Pellet-Many, C., Jones, T., Mahmoud, M. and Zachary, I. (2018). VEGF (Vascular Endothelial Growth Factor) Induces NRP1 (Neuropilin-1) Cleavage via ADAMs (a Disintegrin and Metalloproteinase) 9 and 10 to Generate Novel Carboxy-Terminal NRP1 Fragments That Regulate Angiogenic Signaling. *Arterioscler. Thromb. Vasc. Biol.* **38**, 1845-1858. doi:10.1161/ATVBAHA.118.311118

Mobley, A. K., Tchaicha, J. H., Shin, J., Hossain, M. G. and McCarty, J. H. (2009). β8 integrin regulates neurogenesis and neurovascular homeostasis in the adult brain. *J. Cell Sci.* **122**, 1842-1851. doi:10.1242/jcs.043257

Moore, R. C., Mastrangelo, P., Bouzamondo, E., Heinrich, C., Legname, G., Prusiner, S. B., Hood, L., Westaway, D., DeArmond, S. J. and Tremblay, P. (2001). Doppel-induced cerebellar degeneration in transgenic mice. *Proc. Natl. Acad. Sci. USA* **98**, 15288-15293. doi:10.1073/pnas.251550798

Nakayama, M., Nakayama, A., van Lessen, M., Yamamoto, H., Hoffmann, S., Drexler, H. C. A., Itoh, N., Hirose, T., Breier, G., Vestweber, D. et al. (2013). Spatial regulation of VEGF receptor endocytosis in angiogenesis. *Nat. Cell Biol.* **15**, 249-260. doi:10.1038/ncb2679

Nishizuka, S. S. and Mills, G. B. (2016). New era of integrated cancer biomarker discovery using reverse-phase protein arrays. *Drug Metab. Pharmacokinet* **31**, 35-45. doi:10.1016/j.dmpk.2015.11.009

Nitta, T., Hata, M., Gotoh, S., Seo, Y., Sasaki, H., Hashimoto, N., Furuse, M. and Tsukita, S. (2003). Size-selective loosening of the blood-brain barrier in claudin-5-deficient mice. *J. Cell Biol.* **161**, 653-660. doi:10.1083/jcb.200302070

Paisley, D., Banks, S., Selfridge, J., McLennan, N. F., Ritchie, A.-M., McEwan, C., Irvine, D. S., Saunders, P. T. K., Manson, J. C. and Melton, D. W. (2004). Male infertility and DNA damage in Doppel knockout and prion protein/Doppel double-knockout mice. *Am. J. Pathol.* **164**, 2279-2288. doi:10.1016/S0002-9440(10)63784-4

Paredes, I., Himmels, P. and Ruiz de Almodóvar, C. (2018). Neurovascular Communication during CNS Development. *Dev. Cell* **45**, 10-32. doi:10.1016/j.devcel.2018.01.023

Pitulescu, M. E. and Adams, R. H. (2014). Regulation of signaling interactions and receptor endocytosis in growing blood vessels. *Cell Adh. Migr.* **8**, 366-377. doi:10.4161/19336918.2014.970010

Posokhova, E., Shukla, A., Seaman, S., Volate, S., Hilton, M. B., Wu, B., Morris, H., Swing, D. A., Zhou, M., Zudaire, E. et al. (2015). GPR124 functions as a WNT7-specific coactivator of canonical beta-catenin signaling. *Cell Rep.* **10**, 123-130. doi:10.1016/j.celrep.2014.12.020

Prusiner, S. B., Stahl, N. and DeArmond, S. J. (1988). Novel mechanisms of degeneration of the central nervous system–prion structure and biology. *Ciba Found Symp.* **135**, 239-260. doi:10.1002/9780470513613.ch16

Prusiner, S. B., Groth, D., Serban, A., Koehler, R., Foster, D., Torchia, M., Burton, D., Yang, S. L. and DeArmond, S. J. (1993). Ablation of the prion protein (PrP) gene in mice prevents scrapie and facilitates production of anti-PrP

antibodies. *Proc. Natl. Acad. Sci. USA* **90**, 10608-10612. doi:10.1073/pnas.90.22.10608

Qin, K., Ding, T., Xiao, Y., Ma, W., Wang, Z., Gao, J. and Zhao, L. (2013). Differential responses of neuronal and spermatogenic cells to the doppel cytotoxicity. *PLoS ONE* **8**, e82130. doi:10.1371/journal.pone.0082130

Rama, N., Dubrac, A., Mathivet, T., Ni Chárthaigh, R.-A., Genet, G., Cristofaro, B., Pibouin-Fragner, L., Ma, L., Eichmann, A. and Chédotal, A. (2015). Slit2 signaling through Robo1 and Robo2 is required for retinal neovascularization. *Nat. Med.* **21**, 483-491. doi:10.1038/nm.3849

Segarra, M., Aburto, M. R., Cop, F., Llaó-Cid, C., Härtl, R., Damm, M., Bethani, I., Parrilla, M., Husainie, D., Schänzer, A. et al. (2018). Endothelial Dab1 signaling orchestrates neuro-glia-vessel communication in the central nervous system. *Science* **361**, eaao2861. doi:10.1126/science.aao2861

Siekmann, A. F., Covassin, L. and Lawson, N. D. (2008). Modulation of VEGF signalling output by the Notch pathway. *BioEssays* **30**, 303-313. doi:10.1002/bies.20736

Silverman, G. L., Qin, K., Moore, R. C., Yang, Y., Mastrangelo, P., Tremblay, P., Prusiner, S. B., Cohen, F. E. and Westaway, D. (2000). Doppel is an N-glycosylated, glycosylphosphatidylinositol-anchored protein. Expression in testis and ectopic production in the brains of Prnp(0/0) mice predisposed to Purkinje cell loss. *J. Biol. Chem.* **275**, 26834-26841. doi:10.1074/jbc.M003888200

Stenman, J. M., Rajagopal, J., Carroll, T. J., Ishibashi, M., McMahon, J. and McMahon, A. P. (2008). Canonical Wnt signaling regulates organ-specific assembly and differentiation of CNS vasculature. *Science* **322**, 1247-1250. doi:10.1126/science.1164594

Swan, R., Kim, S. J., Campbell, J. P., Paul Chan, R. V., Sonmez, K., Taylor, K. D., Li, X., Chen, Y.-D. I., Rotter, J. I., Simmons, C. et al. (2018). The genetics of retinopathy of prematurity: a model for neovascular retinal disease. *Ophthalmol Retina* **2**, 949-962. doi:10.1016/j.oret.2018.01.016

Tam, S. J. and Watts, R. J. (2010). Connecting vascular and nervous system development: angiogenesis and the blood-brain barrier. *Annu. Rev. Neurosci.* **33**, 379-408. doi:10.1146/annurev-neuro-060909-152829

Tamgüney, G., Giles, K., Glidden, D. V., Lessard, P., Wille, H., Tremblay, P., Groth, D. F., Yehiely, F., Korth, C., Moore, R. C. et al. (2008). Genes contributing to prion pathogenesis. *J. Gen. Virol.* **89**, 1777-1788. doi:10.1099/vir.0.2008/001255-0

Tata, M., Ruhrberg, C. and Fantin, A. (2015). Vascularisation of the central nervous system. *Mech. Dev.* **138**, 26-36. doi:10.1016/j.mod.2015.07.001

Vanhollebeke, B., Stone, O. A., Bostaille, N., Cho, C., Zhou, Y., Maquet, E., Gauquier, A., Cabochette, P., Fukuhara, S., Mochizuki, N. et al. (2015). Tip cell-specific requirement for an atypical Gpr124- and Reck-dependent Wnt/β-catenin pathway during brain angiogenesis. *eLife* **4**, e06489. doi:10.7554/eLife.06489

Visel, A., Thaller, C. and Eichele, G. (2004). GenePaint.org: an atlas of gene expression patterns in the mouse embryo. *Nucleic Acids Res.* **32**, 552D-556D. doi:10.1093/nar/gkh029

Watts, J. C. and Westaway, D. (2007). The prion protein family: diversity, rivalry, and dysfunction. *Biochim. Biophys. Acta* **1772**, 654-672. doi:10.1016/j.bbadis.2007.05.001

Zhao, Z., Nelson, A. R., Betsholtz, C. and Zlokovic, B. V. (2015). Establishment and dysfunction of the blood-brain barrier. *Cell* **163**, 1064-1078. doi:10.1016/j.cell.2015.10.067